International Journal of Multiphase Flow 195 (2026) 105547

Contents lists available at ScienceDirect

International Journal of Multiphase Flow

journal homepage: www.elsevier.com/locate/ijmulflow

Research Paper

Eliminating gas accumulation in horizontal diverging channels under two-phase flow using upstream solid cross-flow steps

Michael Mansour [a,b,*], Mena Shenouda [b], Nicola Zanini [c], Dominique Thévenin [b]

[a] Mechanical Power Engineering Department, Faculty of Engineering - Mataria, Helwan University, 11718 Cairo, Egypt
[b] Lab. of Fluid Dynamics & Technical Flows, University of Magdeburg "Otto Von Guericke", 39106 Magdeburg, Germany
[c] University of Ferrara - Department of Engineering, Via Saragat 1, 44122 Ferrara, Italy

ARTICLE INFO

Keywords:
Gas–liquid two-phase flow
Gas accumulation
Diverging channels
Cross-flow solid steps
Pressure recovery
Centrifugal pumps

ABSTRACT

Gas accumulation in gas–liquid two-phase flows creates major challenges in centrifugal pumps and diverging channels, as trapped gas in low-pressure separation zones promotes flow separation, reduces pressure recovery, and increases the risk of system failure. To address this, the present study proposes a novel and simple passive control strategy using upstream cross-flow solid steps of varying heights (2, 5, and 8 mm) in a horizontal diverging channel. Controlled experiments combining Laser Doppler Anemometry (LDA), high-speed imaging, and pressure measurements were performed to evaluate the effect of step height on flow separation, bubble behavior, and pressure recovery. Results show that steps of 5 mm and 8 mm could successfully eliminate gas accumulation and significantly improve pressure recovery compared to the baseline without steps, while the 2 mm step had only a marginal effect. These improvements are attributed to enhanced bubble breakup, increased vertical dispersion, and elevated turbulence, while reducing flow separation. The findings not only provide benchmark data for validating two-phase flow models but also offer practical design guidelines for improving gas handling in centrifugal pumps and related industrial systems.

1. Introduction

Gas–liquid two-phase flows play a crucial role in diverse engineering and industrial applications, including nuclear reactor cooling, oil–gas transportation, wastewater treatment, solar collectors, chemical reactors, oil wells, refrigeration systems, heat exchangers, and energy storage technologies (Mansour et al., 2018b; Brennen, 2005; Sharma et al., 2009; Chen et al., 2009; Ewing et al., 1999). These flows exhibit behavior that differs significantly from single-phase flows, even at low gas fractions. The central challenge lies in capturing the complex interplay between liquid and gas phases, which often features unsteady dynamics, rapid flow-pattern transitions, and strong interfacial interactions. Additionally, flow separation and recirculation zones can induce gas build-up, reducing overall performance, and compromising system stability (Mansour and Thévenin, 2023; Ishii and Hibiki, 2010; Manzano Ruiz, 1980; Hundshagen and Skoda, 2023; Mansour et al., 2022, 2018c; Barrios and Prado, 2011; Zhu et al., 2008).

Gas accumulation is a critical concern in two-phase gas–liquid flow systems, particularly in diverging flow passages such as diffusers and impeller channels of centrifugal pumps. The expanding cross-sectional area in these geometries promotes flow separation and recirculation, creating favorable conditions for bubble coalescence and localized gas entrapment. In centrifugal pumps, these gas pockets can significantly degrade hydraulic performance, causing a sharp drop in head and efficiency even at low gas volume fractions (1%). At higher gas contents, flow instabilities intensify, and "gas-locking" may occur, where trapped gas obstructs impeller passages, potentially leading to complete pump failure (Manzano Ruiz, 1980; Poullikkas, 1992, 2003; Noghrehkar et al., 1995; Caridad et al., 2008; Campo and Chisely, 2010). While pumps perform reliably with single-phase liquids, their performance deteriorates rapidly under two-phase conditions (Amoresano et al., 2014; Zhu et al., 2017; Monte Verde et al., 2017; Mansour et al., 2018b,c). Thus, mitigating gas buildup in diverging sections remains a central challenge in two-phase flow research, necessitating robust experimental investigations and innovative passive control strategies (Mansour et al., 2023).

The problem appears not only in centrifugal pump impellers, but is also encountered in Venturi tubes, pipeline diffusers, and discharge passages of pump stations, where gas accumulation alters critical performance metrics such as pressure recovery (Liu et al., 2020; Huang et al., 2018; Zhao et al., 2018; Yin et al., 2015). However, most prior research on two-phase flows has focused on horizontal rectangular channels with either constant cross-sections (Chen et al., 2009; Aziz

* Corresponding author at: Lab. of Fluid Dynamics & Technical Flows, University of Magdeburg "Otto Von Guericke", 39106 Magdeburg, Germany.
E-mail address: michael.mansour@ovgu.de (M. Mansour).

https://doi.org/10.1016/j.ijmultiphaseflow.2025.105547
Received 5 July 2025; Received in revised form 8 October 2025; Accepted 14 November 2025
Available online 17 November 2025
0301-9322/

Nomenclature

Roman symbols

A_u	Upstream cross-sectional area [m^2]
D_{32}	Sauter mean diameter [mm]
D_{median}	Median diameter [mm]
d_{hd}	Downstream hydraulic diameter [m]
d_{hu}	Upstream hydraulic diameter [m]
I	Light intensity [cd]
L_1	Upstream straight pipe length [m]
L_2	Downstream straight pipe length [m]
P_2	Reference pressure (sensor 2) [mbar]
p	Local pressure [mbar]
Q_G	Gas volume flow rate [L/h]
Q_L	Liquid volume flow rate [m^3/s]
Q_T	Total volume flow rate ($Q_L + Q_G$) [m^3/s]
Re_G	Superficial gas Reynolds number [–]
Re_L	Superficial liquid Reynolds number [–]
u_G	Superficial gas velocity [m/s]
u_L	Superficial liquid velocity [m/s]
x	Axial distance [m]
y	Vertical distance [m]

Greek symbols

$\dot{\varepsilon}$	Gas volume fraction [%]
ρ_G	Density of gas [kg/m^3]
ρ_L	Density of liquid [kg/m^3]
σ	Standard deviation of BSD [mm]
μ_G	Viscosity of gas [Pa s]
μ_L	Viscosity of liquid [Pa s]

Subscripts

G	Gas
hd	Downstream hydraulic diamter
hu	Upstream hydraulic diameter
L	Liquid
u	Upstream

Acronyms

BSD	Bubble size distribution
LDA	Laser Doppler Anemometry
VOF	Volume of Fluid model
LED	Light-emitting diodes
LES	Large Eddy Simulations

et al., 1999; Vallée et al., 2008; Wambsganss et al., 1992) or abrupt geometric transitions such as sudden expansion or contraction (Chen et al., 2009, 2007; Pakhomov and Terekhov, 2022; Abdelall et al., 2005; Ahmed et al., 2008). For example, in previous research (Aloui and Souhar, 1996), two-phase bubbly flow was studied through a sudden expansion, revealing that bubbles are trapped in the large vortex region downstream of the expansion, leading to a maximum local void fraction there. Bubbles follow closed trajectories in this zone, with velocities approaching zero at the vortex center, causing them to accumulate and remain nearly stationary. This accumulation affected pressure recovery significantly. In another recent study (Arabi et al., 2024), it was demonstrated further that larger expansion angles degrade pressure recovery due to increased recirculation and gas accumulation. This confirms the need for passive control strategies to eliminate gas accumulations.

In contrast, gradually diverging channels, especially under two-phase flow conditions, have received comparatively limited attention. Some notable exceptions include investigations into pressure recovery in vertical circular diffusers (Anupriya and Jayanti, 2014) and micro-scale rectangular channels with converging/diverging geometries (Hwang et al., 2005), where the deceleration of gas in the diverging region promoted bubble coalescence and markedly altered flow structures. However, the bulk of existing studies have been restricted to diffusers with constant opening angles, i.e., flat or non-curved test sections (Chen et al., 2009; Pakhomov and Terekhov, 2022; Abdelall et al., 2005; Ahmed et al., 2008; Anupriya and Jayanti, 2014; Hwang et al., 2005; Ding et al., 2021; Eskin and Deniz, 2012; Kourakos et al., 2009; Deniz and Eskin, 2015, 2012), where flow separation is generally limited and substantial gas accumulation is rarely observed. This reveals a clear gap in the literature, since little is known about how gradually diverging channels with continuously increasing opening angles influence flow separation, gas accumulation, and pressure recovery under two-phase flow conditions.

In earlier work (Mansour et al., 2018a), we examined gas–liquid two-phase flow within a horizontal diverging channel featuring a gradually increasing opening angle. The study revealed several mechanisms responsible for gas accumulation and phase segregation. Specifically, large recirculation zones induced by flow separation were found to trap gas bubbles, leading to significant accumulation. As the air flow rate increased, the size of these gas pockets grew steadily. Interestingly, increasing the water flow rate had a non-monotonic effect, where it initially enlarged the gas accumulation due to the expansion of recirculation zones, but further increases in liquid flow reduced accumulation as turbulence intensity rose, which disturbs the accumulated gas. Notably, even at very low gas volume fractions (as little as 0.05%), a substantial air pocket developed near the diffuser outlet, disrupting the velocity field and reducing pressure recovery. The study highlighted key strategies for reducing gas buildup, i.e., primarily by reducing flow separation or enhancing turbulence levels (Mansour et al., 2018a). Nevertheless, this earlier investigation did not attempt to control gas accumulation, leaving open the question of how passive modifications could be used to mitigate such effects.

While numerical simulations have substantially advanced the understanding of two-phase flow behavior, they continue to face notable numerical limitations (Hundshagen et al., 2019; Mansour et al., 2018a; Müller et al., 2015; Kopparthy et al., 2020). The combination of the Reynolds Stress Model (RSM) and the Volume of Fluid (VOF) method demonstrated strong potential in accurately predicting the behavior of gas accumulations (Kopparthy et al., 2020). However, its accuracy diminishes at higher Reynolds numbers, where numerical errors become more pronounced. In contrast, the disperse two-fluid model and associated turbulence closures have, in some cases, failed to capture gas accumulation altogether (Hundshagen et al., 2021). The most reliable predictions have been achieved using a hybrid multiphase framework that integrates Eulerian–Eulerian solvers with enhanced VOF schemes and Large Eddy Simulation (LES) models (Nguyen et al., 2022). This advanced method successfully reproduced key flow features and accurately predicted the location and extent of gas accumulations. Nonetheless, its predictive performance remains highly sensitive to the initial prescribed bubble size, underscoring the necessity for further refinement in two-phase modeling and interfacial dynamics. These modeling shortcomings further highlight the importance of new experimental benchmarks in diverging channels to validate and guide the development of reliable computational approaches.

Our recent investigations introduced thin metal toothed steps with vertical heights of 2, 5, and 8 mm as cross-flow obstacles within a horizontal diverging channel, resulting in moderate reductions of gas accumulation under specific conditions (Mansour et al., 2025a,b). These steps enhanced turbulence intensity, promoting the breakup of larger bubbles into smaller ones and redirecting them toward the channel center, away from gas accumulation zones. While the 2 mm

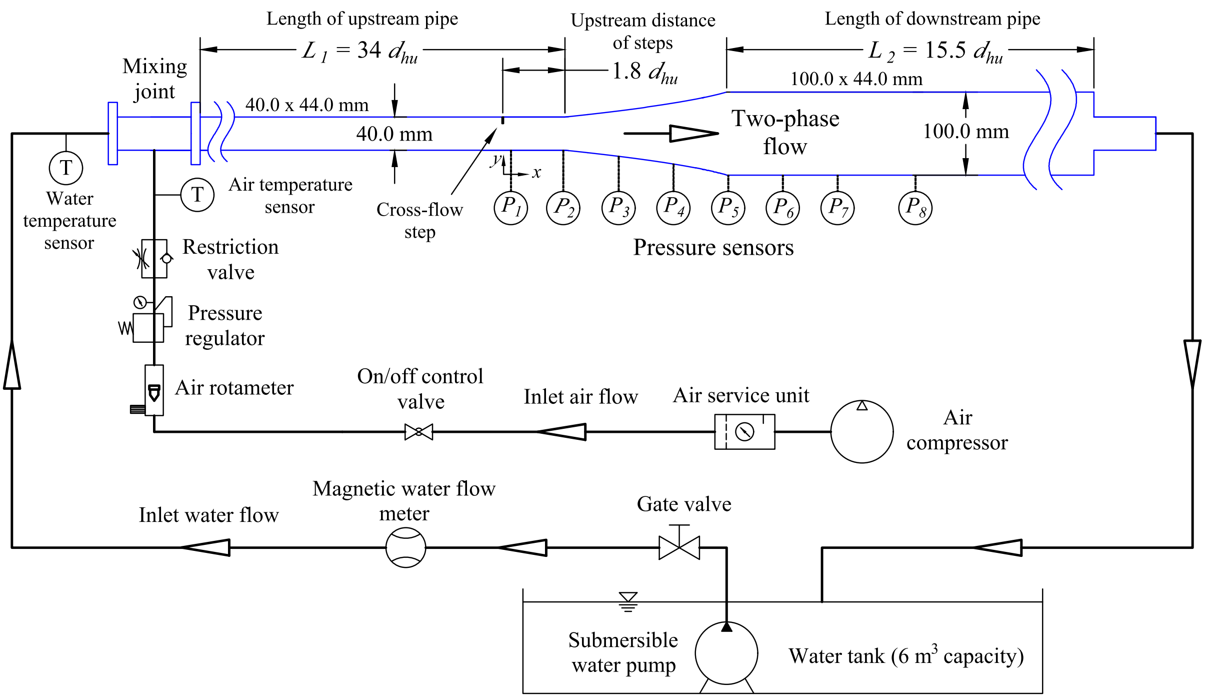

Fig. 1. Schematic diagram showing the details of the experimental setup.

step showed minimal effectiveness, the 5 mm and 8 mm toothed configurations significantly improved bubble dispersion and moderately enhanced pressure recovery. However, a key shortcoming of this approach was its limited performance at low water flow rates, where the toothed steps failed to suppress gas accumulation or improve pressure recovery. This limitation motivates the exploration of alternative passive control designs that remain effective across a broader operating range.

Accordingly, the present study proposes a novel passive control strategy employing upstream solid cross-flow steps. The main objectives are to mitigate gas accumulation and achieve high pressure recovery in the diffuser under various two-phase flow conditions, which was not possible by the strategies and modifications employed before. Three solid metal plates with heights of 2 mm, 5 mm, and 8 mm were installed along the upper wall of the inlet channel and thoroughly investigated. These solid cross-flow steps are designed to enhance turbulence, promote bubble breakup, improve vertical redistribution of bubbles, and reduce flow separation. As a result, they aim to suppress gas accumulation and ensure robust pressure recovery under a wide range of two-phase flow conditions. Building on previous studies (Mansour et al., 2018a; Kopparthy et al., 2020; Nguyen et al., 2022; Hundshagen et al., 2021; Mansour et al., 2025a), the experiments utilized the same diffuser geometry, characterized by a gradually increasing opening angle to induce flow separation and gas accumulation. This simplified diffuser geometry, instead of a full pump system with rotating parts, enables more precise and detailed characterization of the flow. A broad range of liquid and gas flow rates was tested (Re_L = 59530–78330; Re_G = 3–9.25). High-speed imaging was used to capture two-phase flow interactions, including inlet bubble sizes and the formation of accumulated gas pockets.

By employing a novel passive control strategy, this study addresses directly the gaps in the literature, namely the lack of experimental data in gradually diverging geometries, and the limited effectiveness of previous geometry and flow modifications in mitigating gas accumulations. Unlike earlier approaches, which could not eliminate gas accumulation, the innovative strategy proposed here successfully achieves this goal, enabling also the diffuser to deliver excellent two-phase pressure recovery. Furthermore, the results provide a comprehensive validation database for numerical models, thereby improving the predictive accuracy of simulations involving two-phase flows. These findings also inform practical design guidelines aimed at reducing gas accumulation in centrifugal pump impellers, ultimately enhancing pump reliability and performance. The following sections present the experimental setup and measurement techniques, followed by a detailed analysis of velocity fields, bubble size distributions, gas accumulation volumes, and pressure recovery under different step configurations and flow conditions. The paper concludes with a summary of the key findings from this investigation.

2. Details of the experimental methodology

Fig. 1 shows a schematic of the experimental setup, which consists of a diverging flow channel, a fluid circulation loop, and flow control instrumentation. The experiment was conducted in a horizontal diffuser channel specifically designed to investigate gas accumulation under controlled two-phase flow conditions. The channel was positioned horizontally so that gravity acted perpendicular to the main flow direction. This orientation, although not reproducing the Coriolis forces present in impellers, induces lateral buoyancy forces that drive gas migration across the passage. Such cross-passage segregation is also observed in centrifugal pump impellers. By contrast, in vertical channels where gravity acts parallel to the flow, gas primarily rises axially and does not reproduce the lateral accumulation mechanisms of interest. Therefore, the horizontal configuration provides a representative environment for studying gas accumulation mechanisms under conditions that are comparable to those in actual rotating impeller passages (Mansour et al., 2018a; Mansour, 2020; Kopparthy et al., 2020; Nguyen et al., 2022; Hundshagen et al., 2021; Mansour et al., 2025a).

The channel was made of transparent acrylic to allow for clear flow visualization and optical measurements. The channel had a rectangular cross-section that widened from 40×44 mm at the inlet to 100×44 mm at the outlet. These dimensions correspond to hydraulic diameters of d_{hu} = 42 mm upstream and d_{hd} = 61 mm downstream, giving a hydraulic diameter ratio of 1.45. To ensure fully developed flow before the diffuser, the inlet channel length was set to $L_1 = 34d_{hu}$, while the outlet channel length was set to $L_2 = 15.5d_{hu}$. The diffuser walls were shaped to create a gradually widening angle, from 6° up to

16°, to intentionally promote flow separation and gas accumulation since earlier investigations showed that separation is likely to occur when the opening angle exceeds approximately 8° to 10° for a wide range of two-phase flow conditions (Mansour et al., 2018a; Mansour, 2020). Therefore, the considered diffuser ensures the occurrence of flow separation, providing a meaningful window for systematically investigating flow separation and gas accumulation under different two-phase flow conditions. The contour of the upper curve follows the equation $x = 13.5y - y^2/10 - 230$, where x and y are the axial and vertical coordinates.

Water is circulated from a 6.0 m^3 tank using a submersible pump, with air introduced via 21 uniformly spaced 1.0 mm holes around the circumference of the mixing joint. The water flow rate is measured using an electromagnetic flow meter (Endress+Hauser Promag 30F), with an accuracy of ±0.5% of the reading (RD). Air was injected into the mixing joint of the two phases through 21 equally spaced peripheral holes (each 1.0 mm in diameter) located at the beginning of the upstream pipe. The air flow rate is measured by a rotameter (Yokogawa RGC1263) with an accuracy of ±2.5% RD. Separate Pt100 RTD sensors (Class B) are used to measure the temperatures of water and air before the mixing joint, with a maximum absolute error of ±0.3 K. The air supply line is equipped with a service unit, pressure regulator (maintaining constant supply pressure), control valve, and restriction valve, ensuring stable and accurate air flow. This configuration also ensured a consistent and reproducible air introduction among all tested cases. Due to buoyancy, the air phase rapidly migrates toward the top part of the pipe, as it would do in any pipe found in a corresponding industrial installation. As shown in Fig. 1, eight pressure sensors (Cerabar T PMC131, range: −1 to +1 bar, accuracy: ±0.5% RD) were installed along the test section to capture pressure variations. The overall uncertainty in the pressure measurements was estimated at approximately 2.9% of the reading. The experiments were repeated several times at the initial stage of the measurements to ensure the reliability of all the considered parameters. Additional information concerning the measurement instruments can be found in Mansour et al. (2018a), Mansour (2020), Mansour et al. (2025a).

Single-phase velocity measurements in the upper region of the diffuser were obtained for pure water flow using a two-component Laser Doppler Anemometry (LDA) system (Dantec Dynamics 2D, see Fig. 2(a)). To enable flow tracking, 10 μm hollow glass-sphere particles were added at a concentration of approximately 0.6 L (with a density of 1.0 g/cm^3) to the 6 m^3 water reservoir, corresponding to a mass concentration of 0.1 g/L and a volume fraction of 0.01%. This low concentration provides sufficient scattering for strong LDA signals while having a negligible effect on the flow. An automated traversing mechanism was employed to collect velocity data at 325 grid points, with a horizontal spacing of 10 mm and a vertical spacing of 7.5 mm, along the midplane of the diffuser (see Fig. 2(b)). At each point, 25,000 velocity samples were recorded at an average sampling frequency of 1.5 kHz to ensure statistical convergence in the turbulent flow regime. The LDA system measures the frequency shift of scattered laser light from the seeding particles. The system emits four intersecting laser beams (two for each velocity component), creating an interference pattern of bright and dark fringes in the measurement volume. When a seeding particle passes through this volume, it scatters light, and the detector measures the Doppler frequency shift of the scattered light. This frequency shift is directly proportional to the velocity of the particle as it passes through the fringes. The software of Dantec Dynamics 2D system automatically processes this frequency shift to calculate the local velocity components from the ensemble-average of the 25,000 velocity samples. The actual location of each measurement point was carefully calibrated to correct for laser beam refraction through the acrylic walls and water interface, as detailed in Mansour (2020). The combined uncertainty in velocity measurements, accounting for sampling, grid resolution, and calibration, was less than 0.5%. The velocity fields were subsequently analyzed using a visualization software (ParaView).

Gas accumulation sizes were determined using shadowgraphy imaging captured by a high-speed camera, with the test section illuminated from behind by two LED panels (see Fig. 2(c)). This arrangement provided clear visualization of the air–water interfaces. Additionally, bubble size distributions (BSDs) were measured within a defined region (25 mm length × 40 mm height) upstream of the diffuser using a second high-speed camera as presented in Fig. 2(d). The uncertainty in bubble diameter measurements was below 4.9%. Accurate BSD measurements are critical for validating numerical models, significantly influencing their prediction accuracy (Nguyen et al., 2022). MATLAB-based post-processing of the recorded videos quantified gas accumulation and bubble dispersion patterns across all tested cases.

Three solid step configurations, with heights of 2 mm, 5 mm, and 8 mm, were considered as shown in Fig. 3. These step sizes were selected to represent a progressively increasing blockage ratio relative to the hydraulic diameter, in order to identify the threshold at which step height begins to exert a significant effect on gas accumulation. The dimensions of the cross-flow steps relative to the upstream hydraulic diameter (d_{hu}) are approximately 0.048, 0.12, and 0.2. The flow in the channel without any steps was used as a reference for comparison (see Fig. 3(b)). The steps were fabricated from stainless steel sheets, each with a uniform thickness of 0.5 mm, positioned 1.8 d_{hu} upstream of the diffuser section, with the steps facing upward, as shown in Fig. 3(a). These cross-flow steps provide practical advantages due to their simple geometry, ease of installation, and cost-effectiveness. The experiments systematically varied gas and liquid flow rates to capture the resulting flow behavior. Data collection focused on single-phase velocity fields, gas accumulation zones, and bubble dispersion patterns, with particular emphasis on how each step configuration influenced the overall flow dynamics and pressure recovery within the diffuser.

3. Results and discussion

3.1. Selected flow conditions

Building upon prior investigations (Mansour et al., 2018a; Mansour, 2020; Kopparthy et al., 2020; Hundshagen et al., 2021; Nguyen et al., 2022), this study selected specific flow conditions to systematically examine gas accumulation, covering different sizes and shapes across different flow regimes. Two liquid flow rates (Q_L) and two gas flow rates (Q_G) were varied, leading to two distinct single-phase and four two-phase flow cases as detailed in Table 1. These cases facilitated a comprehensive evaluation of the effects of the inserted solid cross-flow steps.

The superficial Reynolds numbers (Re) for each phase were computed according to Eqs. (1) and (2), where ρ denotes fluid density, μ is the dynamic viscosity, and u represents the superficial inlet velocity calculated via Eqs. (3) and (4), for liquid and gas, respectively. Subscripts L and G refer to the liquid (water) and gas (air) phases, respectively, while A_u corresponds to the upstream channel cross-sectional area. These (superficial) Reynolds numbers characterize the flow regimes by assuming each phase uniformly occupies the channel cross-section. Furthermore, the inlet gas volume fraction ($\dot{\epsilon}$) given in Table 1 for each case was determined based on Eq. (5).

$$\mathrm{Re}_L = \frac{\rho_L u_L d_{hu}}{\mu_L} \quad (1)$$

$$\mathrm{Re}_G = \frac{\rho_G u_G d_{hu}}{\mu_G} \quad (2)$$

$$u_L = \frac{Q_L}{A_u} \quad (3)$$

$$u_G = \frac{Q_G}{A_u} \quad (4)$$

$$\dot{\epsilon} = \frac{Q_G}{Q_G + Q_L} \quad (5)$$

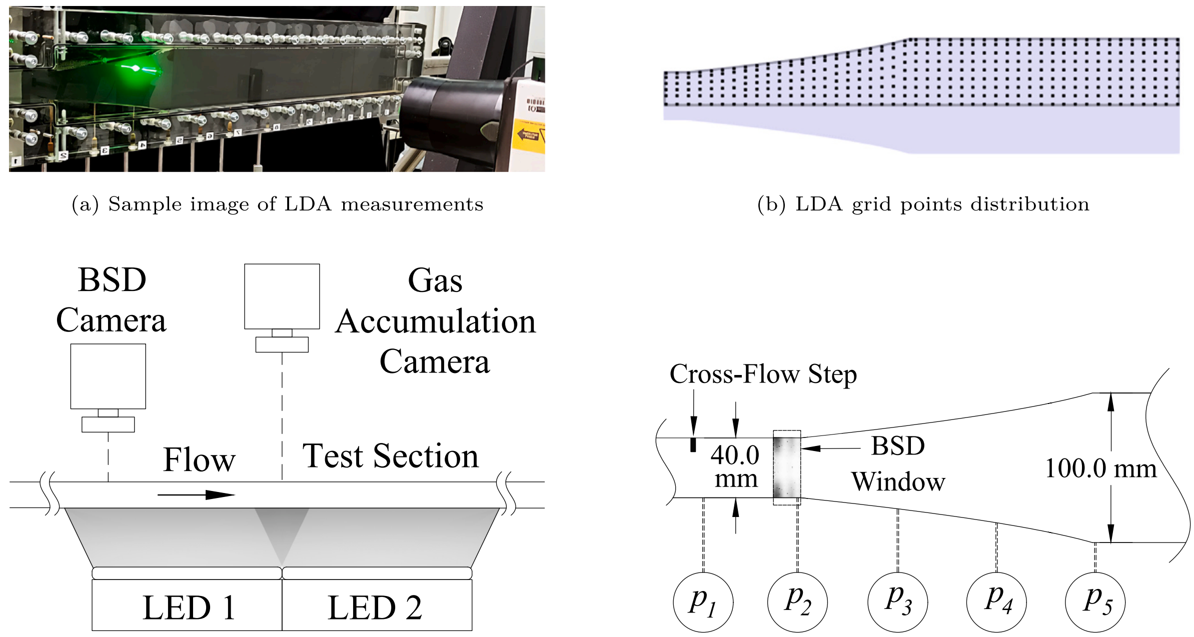

(a) Sample image of LDA measurements
(b) LDA grid points distribution
(c) Top view of shadowgraphy setup
(d) Schematic illustration of BSD window location

Fig. 2. Details of the measurements, (a) Sample image of LDA measurements, (b) LDA grid points distribution, (c) Shadowgraphy setup, and (d) BSD window placement with pressure measurement locations.

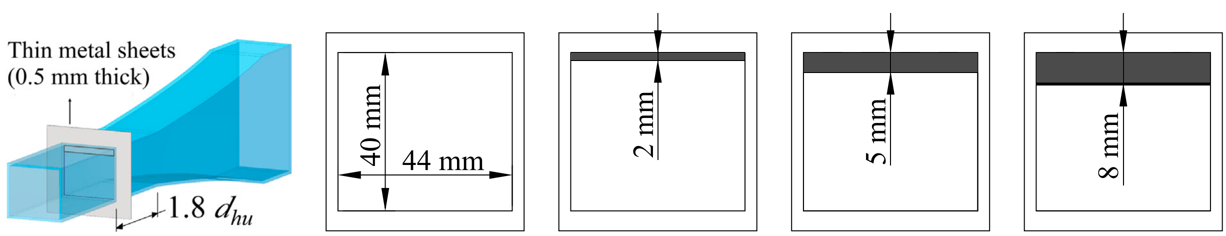

(a) Sheet installation (b) No step (c) 2 mm solid step (d) 5 mm solid step (e) 8 mm solid step

Fig. 3. Installation and dimensions of the considered solid cross-flow steps.

Table 1
Flow conditions examined in this study.

Case#	Flow type	Q_L (m^3/h)	Q_G (L/h)	Re$_L$	Re$_G$	$\dot{\varepsilon}$ (%)
1	Single-phase (water)	9.5	0	59 530	0	0
2	Single-phase (water)	12.5	0	78 330	0	0
3	Two-phase (water–air)	9.5	7.07	59 530	3.10	0.074
4	Two-phase (water–air)	9.5	21.21	59 530	9.25	0.223
5	Two-phase (water–air)	12.5	7.07	78 330	3.10	0.056
6	Two-phase (water–air)	12.5	21.21	78 330	9.25	0.169

To avoid any confusion between air bubbles and vapor cavities, all experiments were conducted under non-cavitating conditions. The minimum cavitation number was evaluated as $C_a \approx 18.5$, substantially exceeding the critical cavitation threshold of $C_{a,crit} = 0.3$, even at peak velocities considering flow fluctuations. Therefore, cavitation was conclusively avoided during all tests.

3.2. Single-phase flow characteristics (flow separation control and turbulence enhancement)

The single-phase flow characteristics play a decisive role in the gas accumulation under two-phase flow conditions. In particular, flow separation in the liquid phase supports gas accumulation, while increased turbulence intensities can reduce the size of gas pockets. The measured velocity magnitude and corresponding velocity fluctuations for all considered configurations are presented in Fig. 4. As shown, flow separation occurs along the upper wall of the diffuser at both flow rates (Re$_L$ = 59530 and Re$_L$ = 78330) in the reference case (without cross-flow steps). The presence of solid steps introduced distinct modifications to the flow structure. The 2 mm step exhibited minimal influence on the flow field compared to the reference, with only slight changes in separation behavior. In contrast, the 5 mm step induced a noticeable upward deflection of the central jet, effectively reducing flow separation along the upper diffuser wall—an area prone to gas accumulation in two-phase flows. The 8 mm step exhibited a similar trend, although it was accompanied by slower velocities near the upper wall. The reduction in flow separation and upward jet deflection observed in the 5 mm and 8 mm cases represent favorable conditions for mitigating gas accumulation under two-phase flow conditions. While the 2 mm step resulted in slightly lower maximum

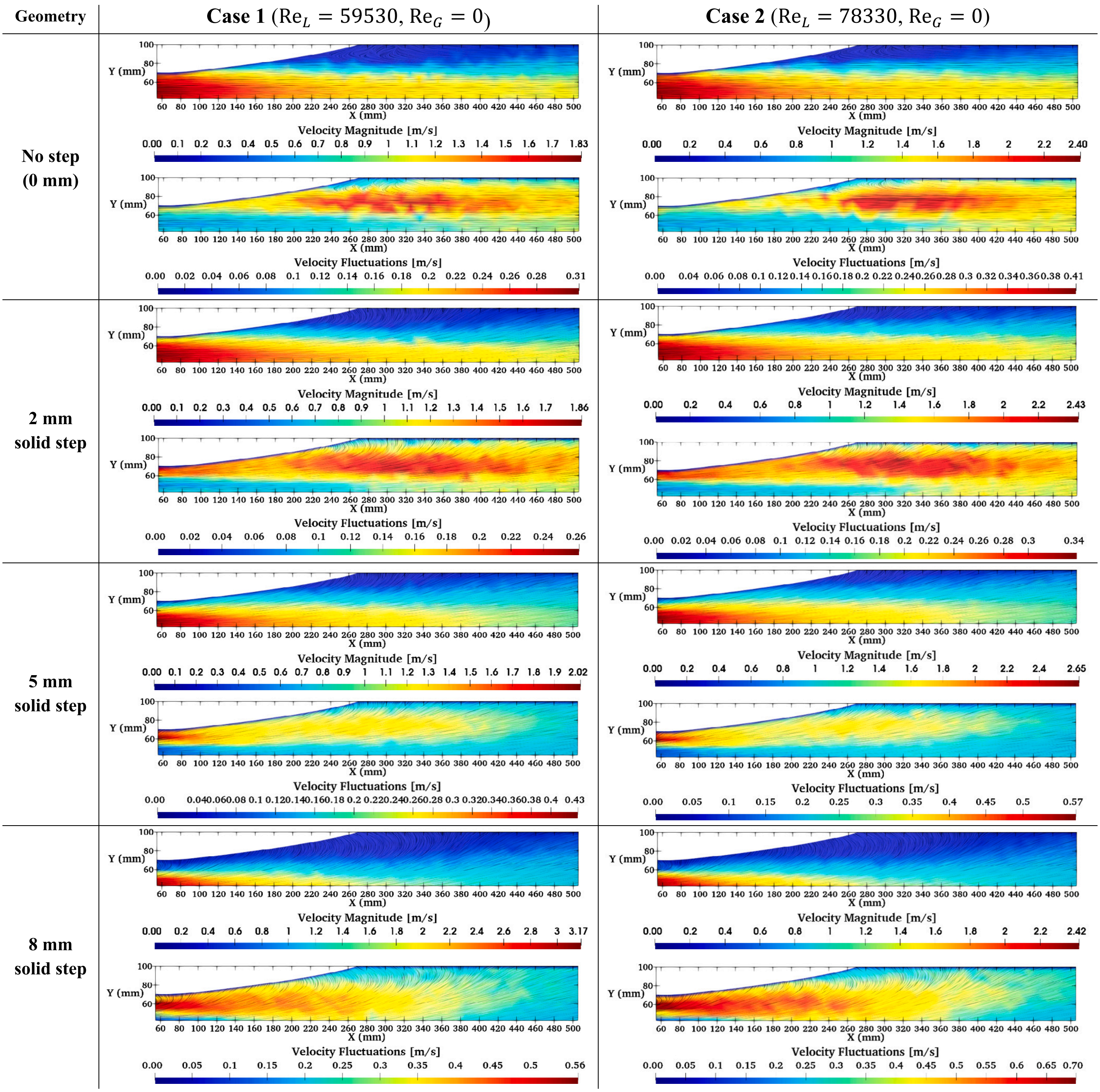

Fig. 4. Single-phase (water) velocity measurements for all configurations at two different water flow rates (Cases 1 and 2).

velocity fluctuations compared to the reference case, the 5 mm and 8 mm steps significantly increased turbulence intensity, as evidenced by higher peak fluctuation values and wider regions of high fluctuations. Notably, the 8 mm step produced the highest levels of velocity fluctuations, indicating enhanced turbulence generation relative to smaller step heights. This increase in turbulence is advantageous in two-phase flows, as it promotes bubble dispersion and suppresses coalescence, emphasizing another advantage of installing the 5 mm and 8 mm solid steps.

3.3. Bubble dispersion and size distribution

Fig. 5 presents high-speed camera images illustrating bubble dispersion patterns for all tested configurations under two-phase flow conditions (Cases 3 to 6). These visualizations highlight the influence of cross-flow solid steps on bubble behavior at the diffuser inlet. The instantaneous images are provided as qualitative examples to illustrate the visual differences in bubble dispersion across various cases and flow conditions. A comprehensive statistical analysis of the bubble size distributions (BSDs) is discussed afterward. For the reference case (without steps), bubbles predominantly accumulate along the upper wall before entering the diffuser. Although slightly smaller bubbles are observed at higher flow rates (Cases 5 and 6), significant coalescence persists.

The 2 mm solid step provides only marginal improvement over the reference case. Under low water flow conditions (Case 4: $Re_L = 59530$, $Re_G = 9.25$), stratified flow patterns are evident downstream of the step, and bubble coalescence is even undesirably increased. This suggests that the 2 mm step height is insufficient to disrupt large bubbles and promote effective dispersion. In contrast, the 5 mm and 8 mm solid

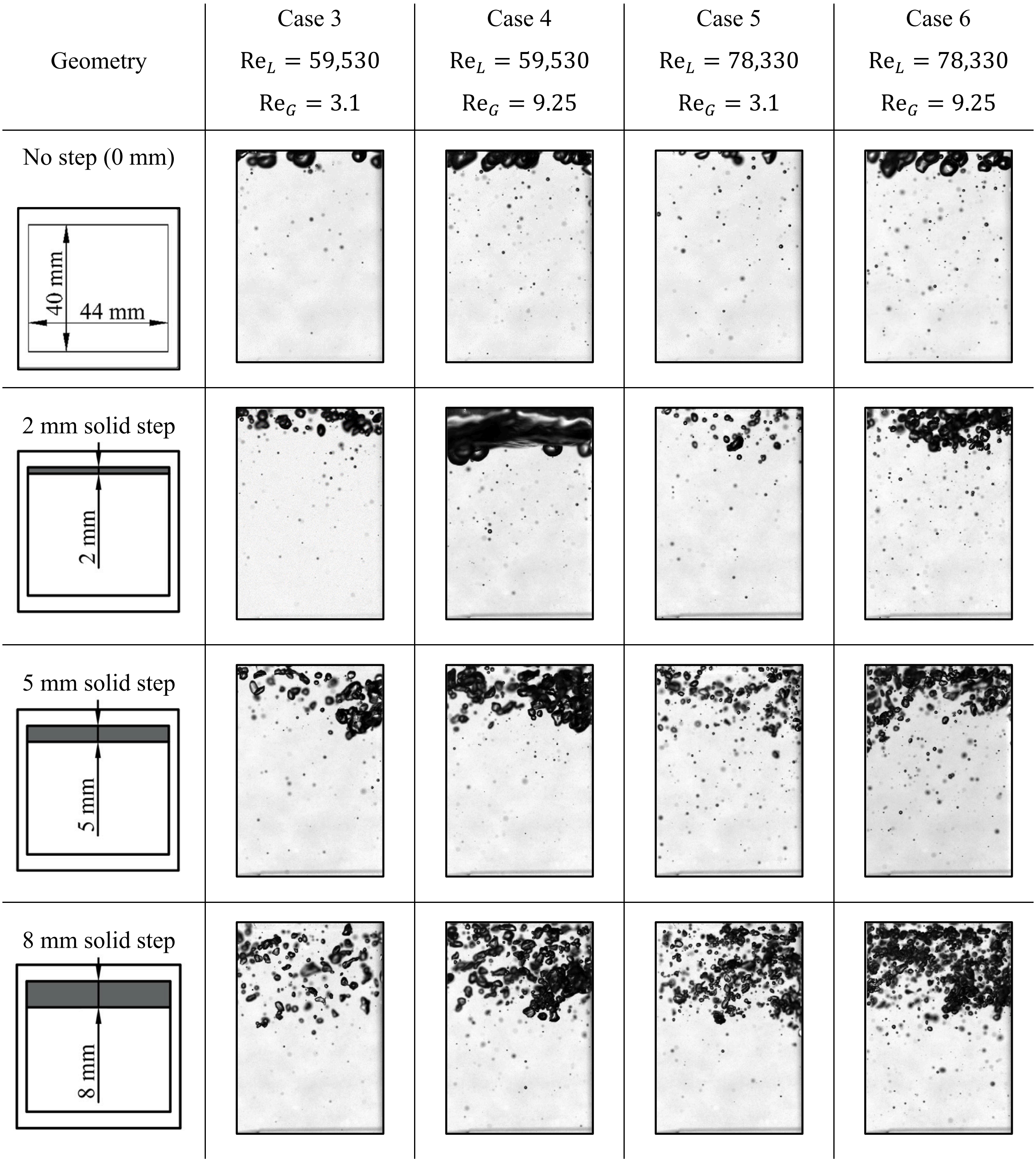

Fig. 5. Bubble dispersion patterns for different steps (0 mm, 2 mm, 5 mm, 8 mm) under two-phase flow conditions.

steps demonstrate substantially improved performance. These configurations induce stronger vertical dispersion and more effective breakup of large bubbles, resulting in finer bubbles and a higher gas–liquid mixing across the inlet channel. The increased step height enhances local turbulence and shear forces, which in turn reduce bubble size and suppress coalescence under all tested flow conditions.

Overall, the results indicate that the effectiveness of cross-flow solid steps in enhancing bubble dispersion is strongly dependent on step height. Larger steps (5 mm and 8 mm) consistently produce favorable flow structures for two-phase mixing by promoting turbulence and disrupting large gas structures.

Accurately capturing bubble size distributions (BSDs) is essential for reliable force estimations, such as drag force, in multiphase flow models and plays a critical role in validating numerical simulations, as bubble size directly affects prediction accuracy (Nguyen et al., 2022). In this study, image processing was applied to 500 high-speed frames recorded at 50 Hz to evaluate BSDs for a sample two-phase flow condition. Key statistical parameters extracted include the median diameter (D_{median}),

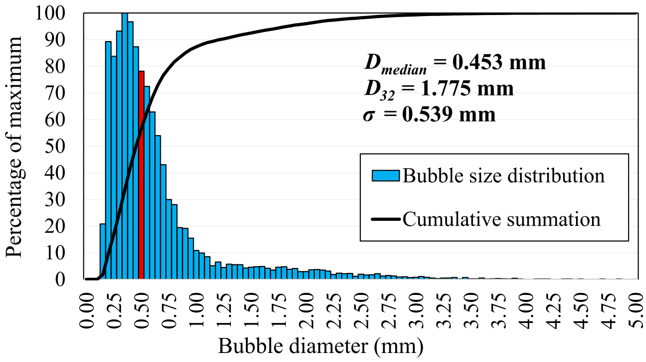

(a) Reference case (without steps) at Case 5

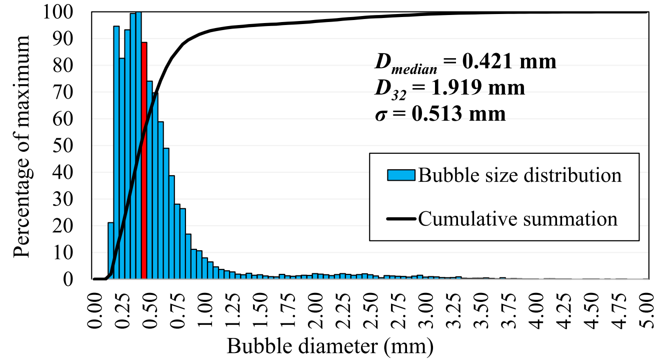

(b) Reference case (without steps) at Case 6

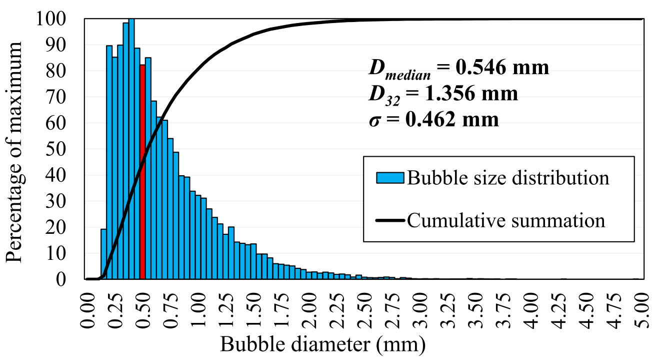

(c) 2 mm solid step at Case 5

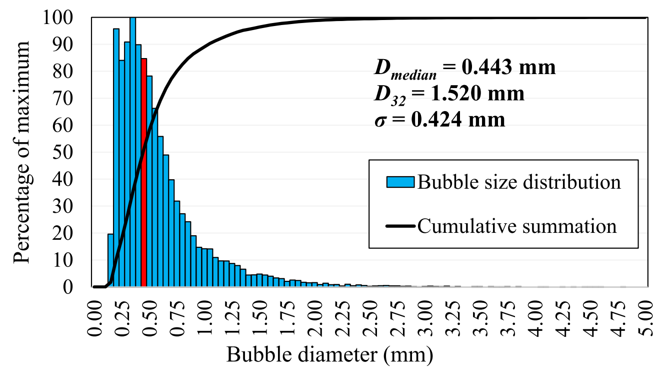

(d) 2 mm solid step at Case 6

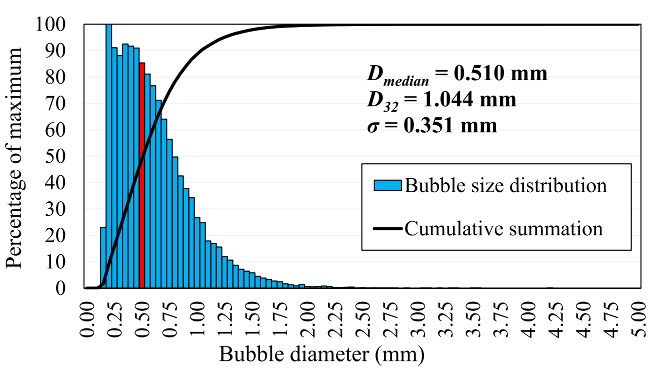

(e) 5 mm solid step at Case 5

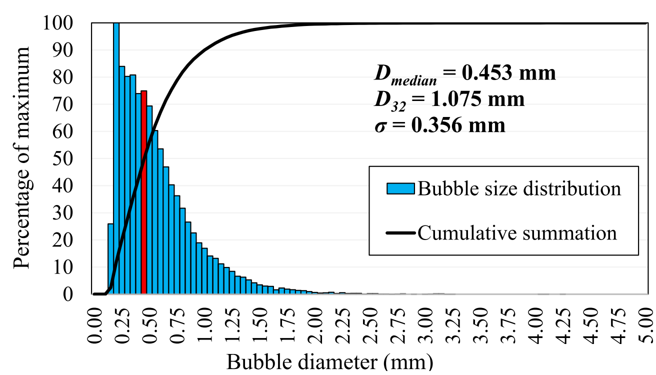

(f) 5 mm solid step at Case 6

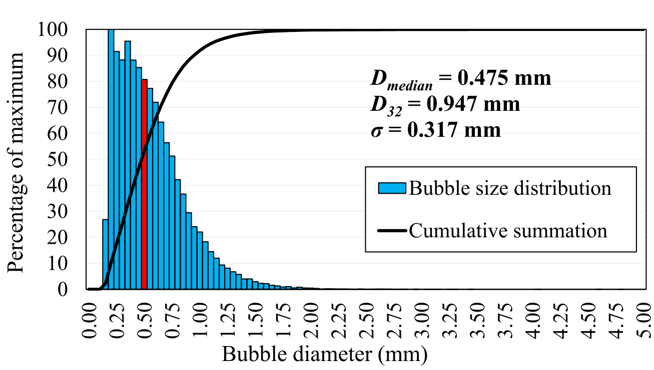

(g) 8 mm solid step at Case 5

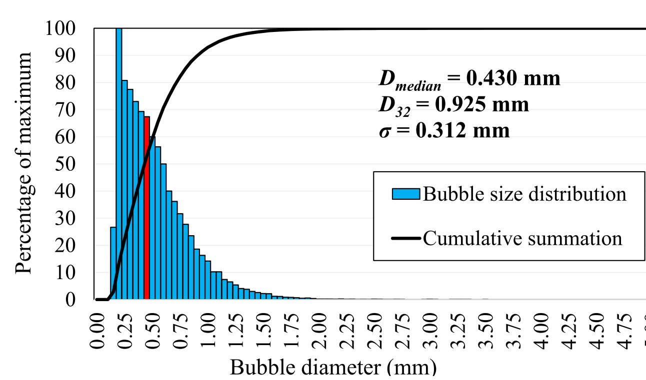

(h) 8 mm solid step at Case 6

Fig. 6. Bubble Size Distributions (BSDs) of all configurations for Case 5 and Case 6.

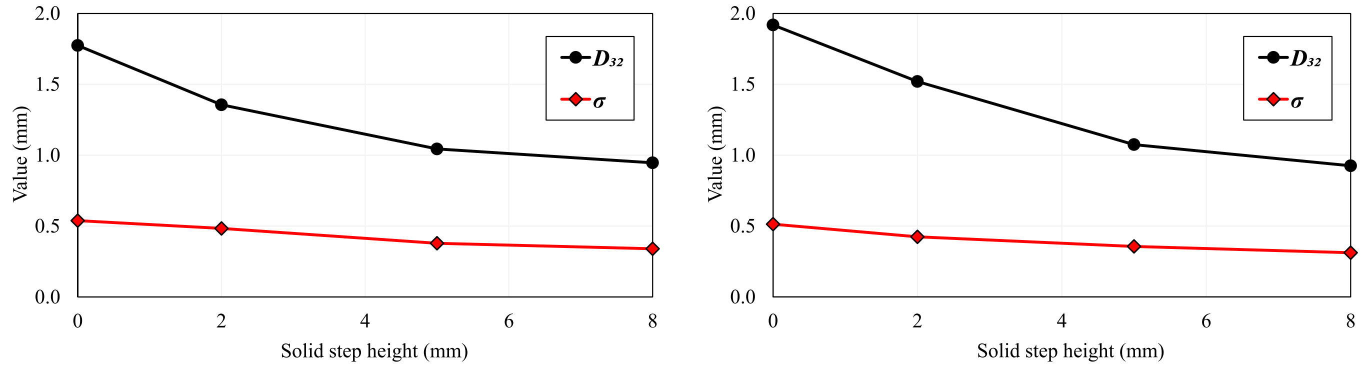

(a) Case 5

(b) Case 6

Fig. 7. Comparison of Sauter mean diameters (D_{32}) and standard deviations (σ) of the bubble size distributions for Case 5 and Case 6 across all tested configurations.

Sauter mean diameter (D_{32}), and standard deviation (σ). The median diameter represents the midpoint of the size distribution, while the Sauter mean diameter, defined as the ratio of total bubble volume to total surface area, serves as a representative measure of the effective bubble size, particularly relevant when assessing interfacial dynamics.

The bubble size distributions were obtained using the particle sizing module of the Davis 8.4 software (LaVision GmbH). The recorded high-speed images were processed using an adaptive thresholding and contour-detection algorithm implemented in the software. Each bubble was identified by fitting an equivalent ellipse to its projected area, from which the equivalent spherical diameter was calculated. This approach accounts for irregular bubble profiles by using area-based diameters rather than assuming circular shapes. To minimize the influence of overlapping bubbles, size recognition was based on local intensity gradients and shape segmentation routines embedded in the Davis particle sizing algorithm. Only bubbles fully within the field of view (with sharp contours) were considered in the statistics, and out-of-focus or poorly resolved detections were discarded. For each test condition, more than 10^4 bubbles were analyzed to ensure statistical convergence of the size distribution.

A quantitative BSD analysis for Case 5 ($\mathrm{Re}_L = 78330$, $\mathrm{Re}_G = 3.1$) and Case 6 ($\mathrm{Re}_L = 78330$, $\mathrm{Re}_G = 9.25$) revealed that the median bubble diameter remained relatively constant across all configurations ($D_{\mathrm{median}} = 0.5\,\mathrm{mm}$), as shown in Fig. 6. However, both the Sauter mean diameter (D_{32}) and standard deviation (σ) decreased notably with increasing step height, indicating narrower and finer size distributions. The 8 mm solid step yielded the most favorable results (see Figs. 6(g) and 6(h)), confirming its superior performance in enhancing bubble breakup and homogenizing the dispersion.

Fig. 7 presents a comparative analysis of the Sauter mean diameter (D_{32}) and standard deviation (σ) for all step configurations, including the reference case. A clear monotonic decrease in both parameters is observed with increasing the solid step height, underscoring the effectiveness of the cross-flow steps in enhancing bubble breakup and promoting finer, more uniform dispersion.

3.4. Gas accumulation performance

This section examines the patterns of gas accumulation and the effectiveness of solid cross-flow steps in mitigating these accumulations under various two-phase flow conditions. Fig. 8 presents representative averaged images of gas accumulation for different test cases, highlighting the influence of liquid and gas superficial Reynolds numbers as well as geometric modifications.

The size and shape of the accumulated gas, as illustrated in Fig. 8, are primarily influenced by the superficial Reynolds numbers of both the liquid and gas phases. In the reference diffuser without steps, large gas pockets accumulate typically near the upper surface of the diffuser inlet. The most substantial accumulation was observed in Case 4 (low water flow, high gas flow), whereas Case 5 (high water flow, low gas flow) exhibited the smallest accumulation.

Commonly, introducing the solid cross-flow steps proved effective in reducing gas accumulation, with performance improving as the step height increased. The 2 mm solid step produced only minor improvements over the baseline, leaving considerable gas retention under most flow conditions. In contrast, the 5 mm and 8 mm steps led to substantial reductions in gas accumulation by suppressing flow separation and enhancing turbulence. These steps effectively eliminated the formation of large gas pockets across all tested flow conditions.

It should be noted that, throughout the experiments, the accumulated air consistently extended across the entire width of the channel, with only brief transient fluctuations observed during the initial stages of accumulation. To determine the average gas accumulation pattern, grayscale images were averaged from 1500 instantaneous frames recorded at 50 Hz, yielding a stable depiction of the air–water interface. These time-averaged images were then binarized using an intensity threshold to delineate the gas boundary. A MATLAB script from (Mansour, 2020) was used to extract the boundary pixels and calculate mean gas boundaries, which are shown as thin white lines in Fig. 9. The full image processing methodology is provided in Mansour (2020).

To further evaluate the effectiveness of the cross-flow steps in reducing gas buildup, the gas void fraction was calculated and compared across all tested configurations. This metric provides a quantitative measure of the amount of gas trapped within the diffuser relative to its total volume. Fig. 10 presents the gas void fraction for each configuration, calculated by dividing the average trapped gas volume by the channel volume measured from the diffuser inlet. This analysis reveals the impact of step height on gas accumulation. As shown, the 2 mm step resulted in only minor reductions compared to the baseline case, indicating limited effectiveness under most conditions. In contrast, the 5 mm and 8 mm steps produced substantial reductions in gas void fraction, highlighting their benefits. For instance, the 8 mm step achieved reductions in void fraction ranging from 92% to 95% in Cases 3 to 6. Maximum effectiveness was recorded in Case 6, which featured the highest Reynolds numbers, with a 95% reduction. This superior performance is attributed to the ability of these steps to generate strong turbulence, facilitate efficient bubble breakup, and minimize the flow separation simultaneously, thereby preventing the formation of large gas regions.

3.5. Analysis of pressure recovery

In this final section, pressure measurements along the diffuser are presented in Fig. 11 to evaluate the impact of step geometry on pressure

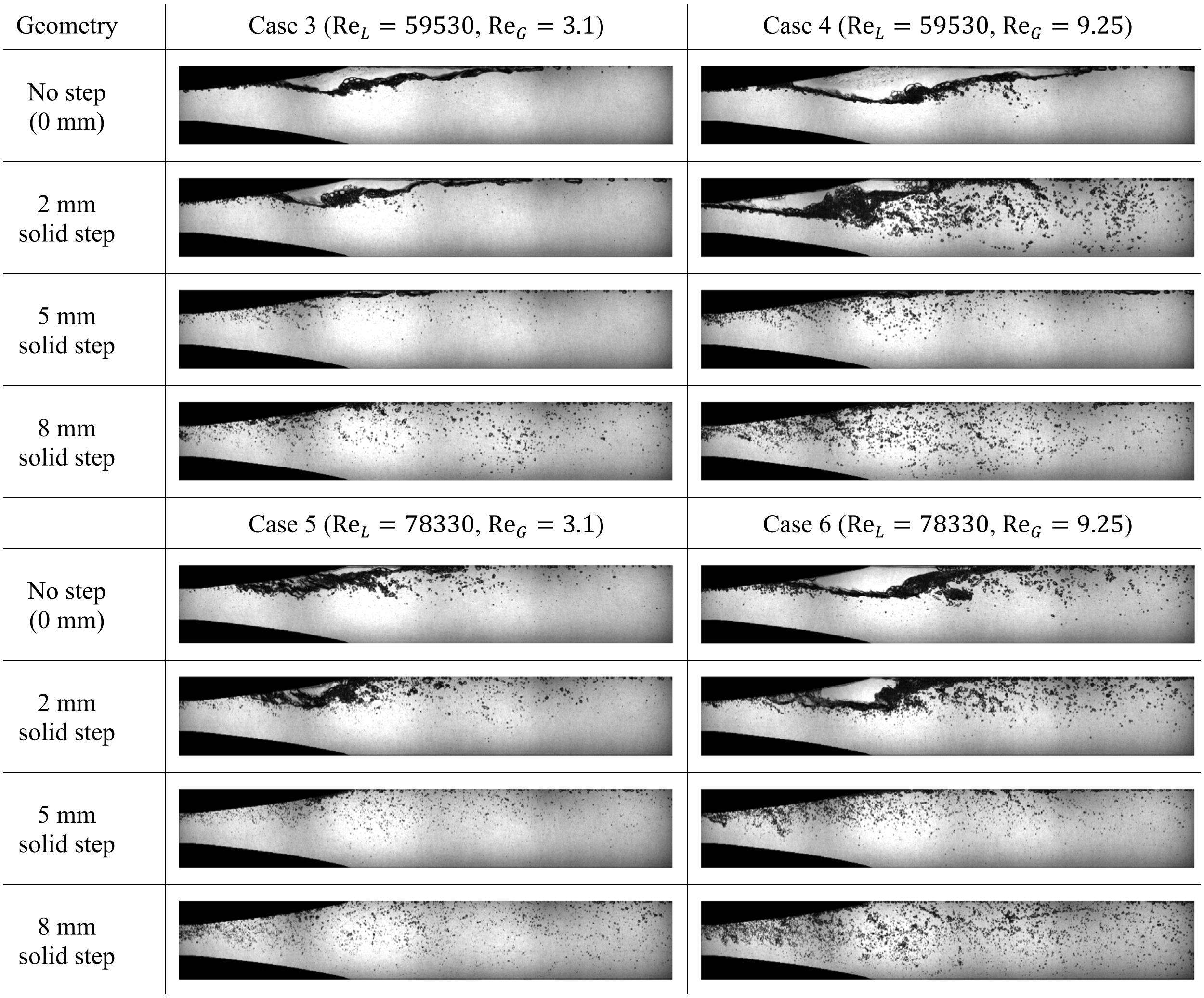

Fig. 8. Gas accumulation patterns for various configurations under different two-phase flow conditions.

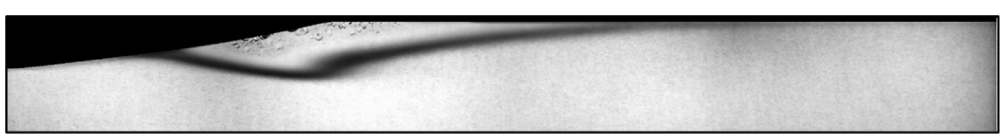

(a) Grayscale averaged image for gas pocket quantification

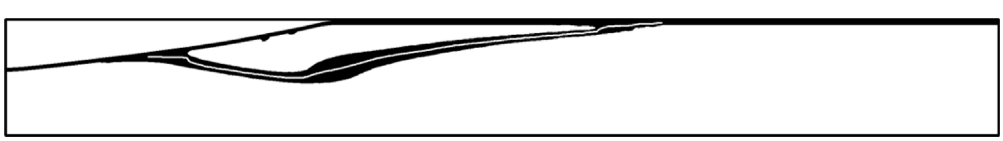

(b) Binarization output with mean gas boundary shown as thin white line

Fig. 9. Processed images used for quantifying the gas accumulation (Case 3).

recovery under various two-phase flow conditions. Pressure sensor 2, located at the diffuser inlet ($x = 0$), served as the reference point for differential pressure calculations. The measured pressure differences were normalized by the maximum single-phase pressure drop ($p_8 - p_2$) recorded in each corresponding test to allow for meaningful comparisons. Pressure data were recorded continuously for 15 min at a sampling rate of 8 Hz, under both single-phase and two-phase flow conditions. To ensure reliability, each test was repeated at least three times, and average values were computed. Under single-phase flow conditions ($Re_G = 0$), the reference diffuser without steps exhibited a steady pressure recovery along the channel, providing a benchmark for evaluating the influence of gas on pressure dynamics. The introduction of gas significantly affected pressure recovery, with reductions observed as gas content increased. This effect was more pronounced at the lower liquid Reynolds number ($Re_L = 59530$) than at the higher value ($Re_L = 78330$), underscoring the adverse impact of gas accumulation on diffuser efficiency, as illustrated in Fig. 11.

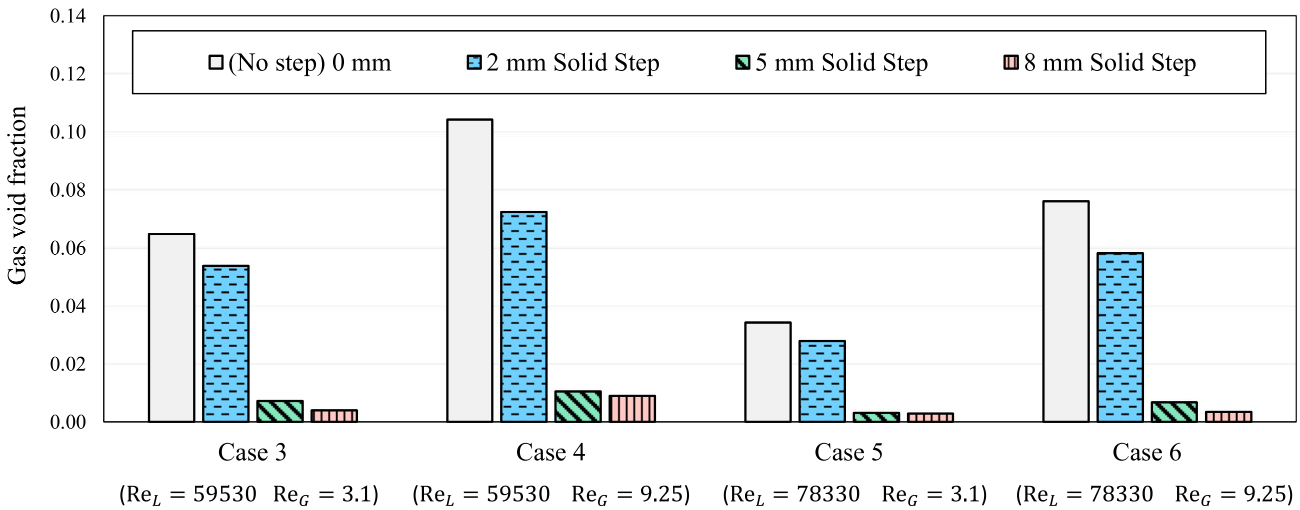

Fig. 10. Gas void fractions for all considered cases.

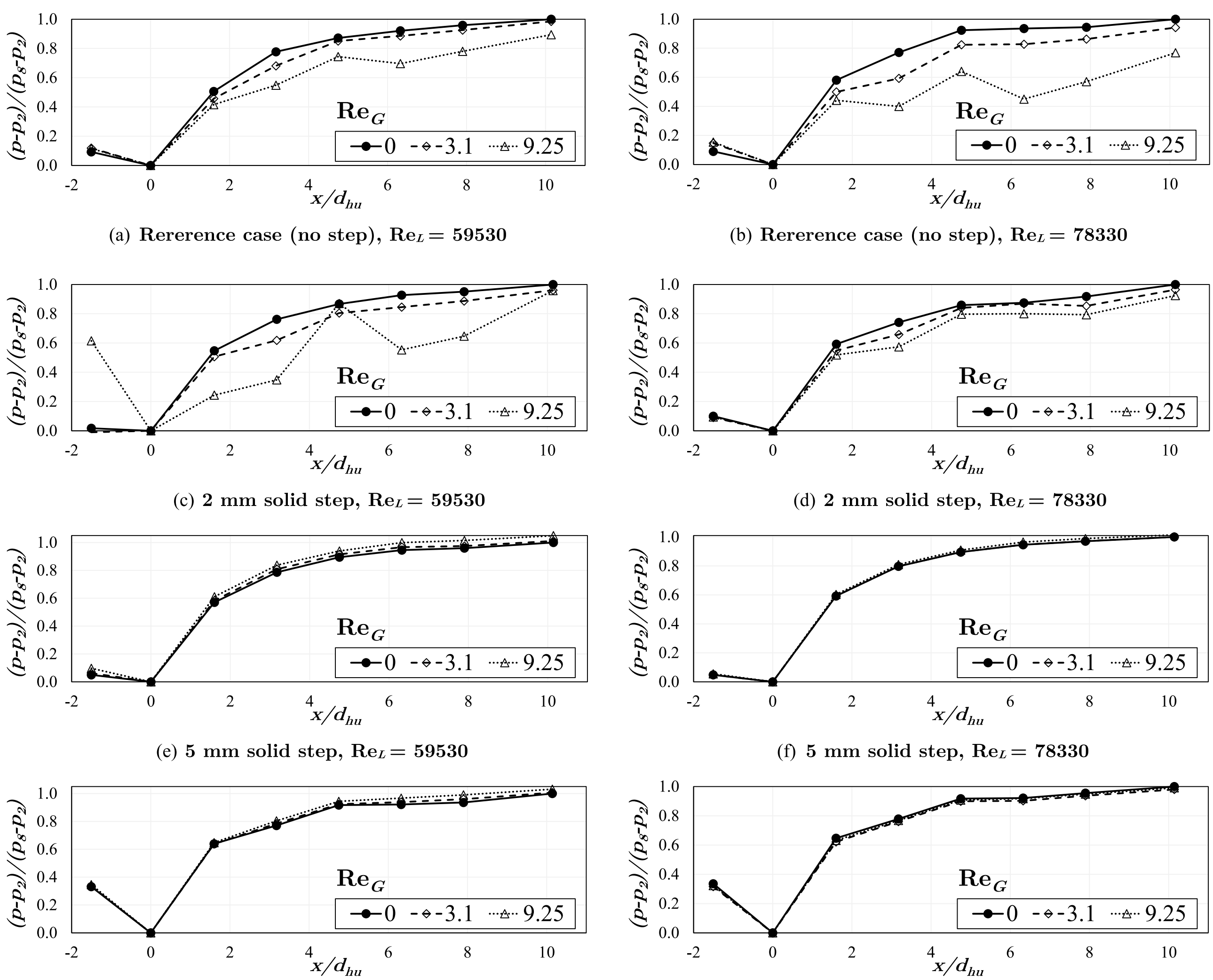

(a) **Rererence case (no step), Re$_L$ = 59530**

(b) **Rererence case (no step), Re$_L$ = 78330**

(c) **2 mm solid step, Re$_L$ = 59530**

(d) **2 mm solid step, Re$_L$ = 78330**

(e) **5 mm solid step, Re$_L$ = 59530**

(f) **5 mm solid step, Re$_L$ = 78330**

(g) **8 mm solid step, Re$_L$ = 59530**

(h) **8 mm solid step, Re$_L$ = 78330**

Fig. 11. Comparative pressure recovery for solid steps across single and two-phase flow conditions.

Pressure recovery profiles varied noticeably among the three solid step configurations. The 2 mm step does not yield any significant improvement compared to the reference case. Additionally, it showed inconsistent performance at $\mathrm{Re}_L = 59530$ with $\mathrm{Re}_G = 9.25$ (Case 4), likely due to the formation of stratified flow (see Case 4 in Fig. 5 for the 2 mm step). The 5 mm and 8 mm steps demonstrated excellent pressure recovery, with pressure profiles closely resembling those of single-phase flow across all tested gas flow rates and both liquid Reynolds numbers. This indicates again the effectiveness of the presented passive technique in mitigating gas accumulations and providing excellent and robust pressure recovery even for strongly different single and two-phase flow conditions.

Generally, the presented experimental results for the larger solid cross-flow steps reveal several advantages concerning two-phase flows in diverging channels, including promoted upward flow redirection, reduced flow separation, enhanced vertical bubble dispersion, suppressed bubble coalescence, mitigated gas accumulation, and significantly improved pressure recovery. This suggests that the considered passive control approach using solid steps could be beneficial not only in diverging channels and pump impeller passages but also in Venturi devices or channels with sudden expansions where gas–liquid separation and coalescence impair performance (Aloui and Souhar, 1996; Arabi et al., 2024; Anupriya and Jayanti, 2014; Hwang et al., 2005; Mansour et al., 2023; Mansour and Thévenin, 2023).

4. Conclusions

This study evaluated the effectiveness of an innovative passive control strategy utilizing upstream cross-flow solid steps (2 mm, 5 mm, and 8 mm) for mitigating gas accumulation and enhancing pressure recovery in a horizontal diverging channel under various two-phase flow conditions. The experimental findings demonstrated that both the presence and height of the solid steps had a pronounced influence on flow behavior, bubble dispersion, and overall diffuser performance. Laser Doppler Anemometry (LDA) confirmed that these steps induced stronger turbulence and greater velocity fluctuations, which facilitated more effective bubble dispersion. Among the tested configurations, the 5 mm and 8 mm steps could substantially promote upward flow redirection, and suppress flow separation along the upper diffuser wall. In contrast, the 2 mm step failed to generate sufficient turbulence, resulting in minimal performance improvement. High-speed shadowgraphy further revealed that the 5 mm and 8 mm steps effectively enhanced vertical bubble dispersion and significantly suppressed bubble coalescence, whereas the 2 mm step had limited impact. As step height increased, both the Sauter mean diameter and standard deviation of the bubble size distributions decreased, indicating finer and more uniform bubble populations. Notably, the 5 mm and 8 mm steps achieved up to 90%–95% reduction in gas accumulation compared to the unmodified diffuser (without cross-flow steps). These modifications also yielded significant improvements in pressure recovery, with the pressure profiles closely matching those observed under single-phase flow, demonstrating near-optimal diffuser performance under all considered two-phase flow conditions. Overall, the results highlight the effectiveness of this novel, passive geometric modification for managing gas–liquid two-phase flows in diffusers. Its simplicity, scalability, and cost-efficiency make it well-suited for industrial implementation, particularly in centrifugal pump systems where gas entrapment can severely impair performance. Moreover, the comprehensive experimental dataset provides a valuable resource for validating numerical models of two-phase flow in geometrically modified channels.

CRediT authorship contribution statement

Michael Mansour: Writing – original draft, Visualization, Validation, Software, Methodology, Investigation, Formal analysis, Data curation, Conceptualization. **Mena Shenouda:** Writing – original draft, Software, Methodology, Investigation, Data curation. **Nicola Zanini:** Writing – review & editing, Visualization, Software, Methodology, Investigation, Data curation. **Dominique Thévenin:** Writing – review & editing, Supervision, Resources, Project administration, Funding acquisition.

Declaration of competing interest

The authors declare the following financial interests/personal relationships which may be considered as potential competing interests: Dominique Thevenin reports financial support was provided by VDMA (Verband Deutscher Maschinen- und Anlagenbau) and BMWi (German Federal Ministry for Economic Affairs and Energy). If there are other authors, they declare that they have no known competing financial interests or personal relationships that could have appeared to influence the work reported in this paper.

Acknowledgments

This research was supported by the VDMA (Verband Deutscher Maschinen- und Anlagenbau) and the BMWi (German Federal Ministry for Economic Affairs and Energy), Germany under grant number IGF 23051. The authors gratefully acknowledge their funding and support.

Data availability

Data will be made available on request.

References

Abdelall, F.F., Hahn, G., Ghiaasiaan, S.M., Abdel-Khalik, S.I., Jeter, S.S., Yoda, M., Sadowski, D.L., 2005. Pressure drop caused by abrupt flow area changes in small channels. Exp. Therm. Fluid Sci. 29 (4), 425–434. http://dx.doi.org/10.1016/j.expthermflusci.2004.05.001.

Ahmed, W.H., Ching, C.Y., Shoukri, M., 2008. Development of two-phase flow downstream of a horizontal sudden expansion. Int. J. Heat Fluid Flow 29 (1), 194–206. http://dx.doi.org/10.1016/j.ijheatfluidflow.2007.06.003.

Aloui, F., Souhar, M., 1996. Experimental study of a two-phase bubbly flow in a flat duct symmetric sudden expansion—Part 1: Visualization, pressure and void fraction. Int. J. Multiph. Flow 22 (4), 651–665. http://dx.doi.org/10.1016/0301-9322(96)00021-3.

Amoresano, A., Langella, G., Niola, V., Quaremba, G., 2014. Advanced image analysis of two-phase flow inside a centrifugal pump. Adv. Mech. Eng. 6, http://dx.doi.org/10.1155/2014/958320.

Anupriya, S., Jayanti, S., 2014. Experimental and modelling studies of gas–liquid vertical annular flow through a diverging section. Int. J. Multiph. Flow 67, 180–190. http://dx.doi.org/10.1016/j.ijmultiphaseflow.2014.05.009.

Arabi, A., Abdul-Majeed, G.H., Boukrouche, H.B., Larbi, Z., 2024. Pressure recovery model for gas-liquid two-phase flow across sudden expansions. Exp. Comput. Multiph. Flow. 6 (1), 14–27. http://dx.doi.org/10.1007/s42757-023-0160-3.

Aziz, W., Chaturvedi, S., Kheireddine, A., 1999. Thermodynamic analysis of two-component, two-phase flow in solar collectors with application to a direct-expansion solar-assisted heat pump. Energy 24 (3), 247–259. http://dx.doi.org/10.1016/S0360-5442(98)00089-9.

Barrios, L., Prado, M.G., 2011. Experimental visualization of two-phase flow inside an electrical submersible pump stage. J. Energy Resour. Technol. 133 (4), 042901. http://dx.doi.org/10.1115/1.4004966.

Brennen, C.E., 2005. Fundamentals of multiphase flow. Camb. Ltd http://dx.doi.org/10.1017/CBO9780511807169.

Campo, A., Chisely, E.A., 2010. Experimental characterization of two-phase flow centrifugal pumps. In: ASME 2010 Power Conf.. American Society of Mechanical Engineers, pp. 803–816. http://dx.doi.org/10.1115/POWER2010-27048.

Caridad, J., Asuaje, M., Kenyery, F., Tremante, A., Aguillón, O., 2008. Characterization of a centrifugal pump impeller under two-phase flow conditions. J. Pet. Sci. Eng. 63 (1–4), 18–22. http://dx.doi.org/10.1016/j.petrol.2008.06.005.

Chen, I.Y., Liu, C.-C., Chien, K.-H., Wang, C.-C., 2007. Two-phase flow characteristics across sudden expansion in small rectangular channels. Exp. Therm. Fluid Sci. 32 (2), 696–706. http://dx.doi.org/10.1016/j.expthermflusci.2007.09.001.

Chen, I.Y., Tseng, C.-Y., Lin, Y.-T., Wang, C.-C., 2009. Two-phase flow pressure change subject to sudden contraction in small rectangular channels. Int. J. Multiph. Flow 35 (3), 297–306. http://dx.doi.org/10.1016/j.ijmultiphaseflow.2008.10.008.

Deniz, E., Eskin, N., 2012. Experimental and numerical investigation of two-phase flow through enlarging singularity. In: Int. Refrig. Air Cond. Conf.. pp. 1–9.

Deniz, E., Eskin, N., 2015. Hydrodynamic characteristics of two-phase flow through horizontal pipe having smooth expansion. ISI Bilim. Ve Tek. Dergisi-Journal Therm. Sci. Technol. 35 (1), 1–9.

Ding, G., Chen, J., Li, Z., 2021. An investigation on the bubble breakup characteristics by recirculation flow in a venturi channel. In: Proceedings of the Fluids Engineering Division Summer Meeting. http://dx.doi.org/10.1115/FEDSM2021-65716, Volume 3: Fluid Mechanics; Micro and Nano Fluid Dynamics; Multiphase Flow, V003T08A002.

Eskin, N., Deniz, E., 2012. Pressure drop of two-phase flow through horizontal channel with smooth expansion. In: Int. Refrig. Air Cond. Conf.. pp. 1–10.

Ewing, M.E., Weinandy, J.J., Christensen, R.N., 1999. Observations of two-phase flow patterns in a horizontal circular channel. Heat Transf. Eng. 20 (1), 9–14. http://dx.doi.org/10.1080/014576399271682.

Huang, J., Sun, L., Du, M., Mo, Z., Zhao, L., 2018. A visualized study of interfacial behavior of air–water two-phase flow in a rectangular venturi channel. Theor. Appl. Mech. Lett. 8 (5), 334–344. http://dx.doi.org/10.1016/j.taml.2018.05.004.

Hundshagen, M., Mansour, M., Thévenin, D., Skoda, R., 2019. Numerical investigation of two-phase air-water flow in a centrifugal pump with closed or semi-open impeller. In: Proceedings of 13th European Turbomachinery Conference on Turbomachinery Fluid Dynamics and Thermodynamics, ETC 2019. http://dx.doi.org/10.29008/ETC2019-011.

Hundshagen, M., Mansour, M., Thévenin, D., Skoda, R., 2021. 3D simulation of gas-laden liquid flows in centrifugal pumps and the assessment of two-fluid CFD methods. Exp. Comput. Multiph. Flow. 3 (3), 186–207. http://dx.doi.org/10.1007/s42757-020-0080-4.

Hundshagen, M., Skoda, R., 2023. State of the art on two-phase non-miscible liquid/gas flow transport analysis in radial centrifugal pumps part C: CFD approaches with emphasis on improved models. Int. J. Turbomach. Propuls. Power 8 (2), 15. http://dx.doi.org/10.3390/ijtpp8020015.

Hwang, J.J., Tseng, F.G., Pan, C., 2005. Ethanol-CO_2 two-phase flow in diverging and converging microchannels. Int. J. Multiph. Flow 31 (5), 548–570. http://dx.doi.org/10.1016/j.ijmultiphaseflow.2005.01.011.

Ishii, M., Hibiki, T., 2010. Thermo-Fluid Dynamics of Two-Phase Flow. Springer Science & Business Media, http://dx.doi.org/10.1007/978-1-4419-7985-8.

Kopparthy, S., Mansour, M., Janiga, G., Thévenin, D., 2020. Numerical investigations of turbulent single-phase and two-phase flows in a diffuser. Int. J. Multiph. Flow 130, 103333. http://dx.doi.org/10.1016/j.ijmultiphaseflow.2020.103333.

Kourakos, V.G., Rambaud, P., Chabane, S., Pierrat, D., Buchlin, J.M., 2009. Two-phase flow modelling within expansion and contraction singularities. Comput. Methods Multiph. Flow V 63, 27. http://dx.doi.org/10.2495/MPF090031.

Liu, X., Lao, L., Falcone, G., 2020. A comprehensive assessment of correlations for two-phase flow through venturi tubes. J. Nat. Gas Sci. Eng. 78, 103323. http://dx.doi.org/10.1016/j.jngse.2020.103323.

Mansour, M., 2020. Transport of two-phase air-water flows in radial centrifugal pumps (Ph.D. thesis). University of Magdeburg, Germany, http://dx.doi.org/10.25673/32539.

Mansour, M., Kopparthy, S., Thevenin, D., 2022. Investigations on the effect of rotational speed on the transport of air-water two-phase flows by centrifugal pumps. Int. J. Heat Fluid Flow 94, 108939. http://dx.doi.org/10.1016/j.ijheatfluidflow.2022.108939.

Mansour, M., Kopparthy, S.B., Thévenin, D., 2023. Improving air-water two-phase flow pumping in centrifugal pumps using novel grooved front shrouds. Chem. Eng. Res. Des. 197, 173–191. http://dx.doi.org/10.1016/j.cherd.2023.07.019.

Mansour, M., Kováts, P., Wunderlich, B., Thévenin, D., 2018a. Experimental investigations of a two-phase gas/liquid flow in a diverging horizontal channel. Exp. Therm. Fluid Sci. 93, 210–217. http://dx.doi.org/10.1016/j.expthermflusci.2017.12.033.

Mansour, M., Thévenin, D., 2023. State of the art on two-phase non-miscible liquid/gas flow transport analysis in radial centrifugal pumps part b: Review of experimental investigations. Int. J. Turbomach. Propuls. Power 8 (4), 42. http://dx.doi.org/10.3390/ijtpp8040042.

Mansour, M., Wunderlich, B., Thévenin, D., 2018b. Effect of tip clearance gap and inducer on the transport of two-phase air-water flows by centrifugal pumps. Exp. Therm. Fluid Sci. 99, 487–509. http://dx.doi.org/10.1016/j.expthermflusci.2018.08.018.

Mansour, M., Wunderlich, B., Thévenin, D., 2018c. Experimental study of two-phase air/water flows in a centrifugal pump working with a closed or a semi-open impeller. In: ASME Turbo Expo 2018: Turbomachinery Technical Conference and Exposition, Oslo, Norway. http://dx.doi.org/10.1115/GT2018-75380, V009T27A012.

Mansour, M., Zanini, N., Shenouda, M., Pinelli, M., Suman, A., Thévenin, D., 2025a. Minimizing gas accumulation in two-phase flow within a diverging horizontal channel using cross-flow millimeter-size steps. In: Proceedings of 16th European Turbomachinery Conference on Turbomachinery Fluid Dynamics and Thermodynamics, ETC16, Hannover, Germany.

Mansour, M., Zanini, N., Shenouda, M., Pinelli, M., Suman, A., Thévenin, D., 2025b. Reducing gas accumulation in horizontal diffusers under two-phase flow using upstream cross-glow steps. Int. J. Turbomach. Propuls. Power 10 (3), 20. http://dx.doi.org/10.3390/ijtpp10030020.

Manzano Ruiz, J.J., 1980. Experimental and theoretical study of two-phase flow in centrifugal pumps (Ph.D. thesis). Massachusetts Institute of Technology.

Monte Verde, W., Biazussi, J.L., Sassim, N.A., Bannwart, A.C., 2017. Experimental study of gas-liquid two-phase flow patterns within centrifugal pumps impellers. Exp. Therm. Fluid Sci. 85, 37–51. http://dx.doi.org/10.1016/j.expthermflusci.2017.02.019.

Müller, T., Limbach, P., Skoda, R., 2015. Numerical 3D RANS simulation of gas-liquid flow in a centrifugal pump with an Euler-Euler two-phase model and a dispersed phase distribution. In: 11th Eur. Conf. Turbomach. Fluid Dyn. Thermodyn.. Madrid.

Nguyen, B.-D., Popp, S., Hundshagen, M., Skoda, R., Mansour, M., Thévenin, D., Hasse, C., 2022. Large eddy simulations of turbulent gas-liquid flows in a diverging horizontal channel using a hybrid multiphase approach. J. Fluids Eng. 145 (3), 031501. http://dx.doi.org/10.1115/1.4056209.

Noghrehkar, G.R., Kawaji, M., Chan, A.M.C., Nakamura, H., Kukita, Y., 1995. Investigation of centrifugal pump performance under two-phase flow conditions. J. Fluids Eng. 117 (1), 129. http://dx.doi.org/10.1115/1.2816802.

Pakhomov, M.A., Terekhov, V.I., 2022. Modeling of turbulent heat-transfer augmentation in gas-droplet non-boiling flow in diverging and converging axisymmetric ducts with sudden expansion. Energies 15 (16), http://dx.doi.org/10.3390/en15165861.

Poullikkas, A., 1992. Two phase flow and cavitation in centrifugal pump: a theoretical and experimental investigation (Ph.D. thesis). © Andreas Poullikkas, Loughborough University.

Poullikkas, A., 2003. Effects of two-phase liquid–gas flow on the performance of nuclear reactor cooling pumps. Prog. Nucl. Energy 42 (1), 3–10. http://dx.doi.org/10.1016/S0149-1970(03)80002-1.

Sharma, A., Tyagi, V., Chen, C., Buddhi, D., 2009. Review on thermal energy storage with phase change materials and applications. Renew. Sustain. Energy Rev. 13 (2), 318–345. http://dx.doi.org/10.1016/j.rser.2007.10.005.

Vallée, C., Höhne, T., Prasser, H.-M., Sühnel, T., 2008. Experimental investigation and CFD simulation of horizontal stratified two-phase flow phenomena. Nucl. Eng. Des. 238 (3), 637–646. http://dx.doi.org/10.1016/j.nucengdes.2007.02.051.

Wambsganss, M., Jendrzejczyk, J., France, D., Obot, N., 1992. Frictional pressure gradients in two-phase flow in a small horizontal rectangular channel. Exp. Therm. Fluid Sci. 5 (1), 40–56. http://dx.doi.org/10.1016/0894-1777(92)90055-A.

Yin, J., Li, J., Li, H., Liu, W., Wang, D., 2015. Experimental study on the bubble generation characteristics for an venturi type bubble generator. Int. J. Heat Mass Transfer 91, 218–224. http://dx.doi.org/10.1016/j.ijheatmasstransfer.2015.05.076.

Zhao, L., Sun, L., Mo, Z., Tang, J., Hu, L., Bao, J., 2018. An investigation on bubble motion in liquid flowing through a rectangular venturi channel. Exp. Therm. Fluid Sci. 97, 48–58. http://dx.doi.org/10.1016/j.expthermflusci.2018.04.009.

Zhu, J., Guo, X., Liang, F., Zhang, H.-Q., 2017. Experimental study and mechanistic modeling of pressure surging in electrical submersible pump. J. Nat. Gas Sci. Eng. 45, 625–636. http://dx.doi.org/10.1016/j.jngse.2017.06.027.

Zhu, Z., Xie, P., Ou, G., Cui, B., Li, Y., 2008. Design and experimental analyses of small-flow high-head centrifugal-vortex pump for gas-liquid two-phase mixture. Chin. J. Chem. Eng. 16 (4), 528–534. http://dx.doi.org/10.1016/S1004-9541(08)60116-0.